Haji Haji, V., Fekih, A., Monje, C. A. y Asfestani, R. F. (2019). H2, H∞, H2/H∞, and μ-synthesis controllers for the speed and temperature control of a real gas turbine unit in a combined cycle power plant. *Energy Science and Engineering,* 7(5), pp. 2205-2222.

DOI: https://doi.org/10.1002/ese3.425

Received: 14 March 2019 | Revised: 20 June 2019 | Accepted: 18 July 2019

DOI: 10.1002/ese3.425

RESEARCH ARTICLE

Energy Science & Engineering Open Access

H_2, H_∞, H_2/H_∞, and *μ-synthesis* controllers for the speed and temperature control of a real gas turbine unit in a combined cycle power plant

Vahab Haji Haji[1] | **Afef Fekih**[2] | **Concepción Alicia Monje**[3]* | **Ramin Fakhri Asfestani**[4]

[1]Young Researchers and Elite Club, Borujerd Branch, Islamic Azad University, Borujerd, Iran

[2]Electrical and Computer Engineering Department, University of Louisiana at Lafayette, Lafayette, LA, USA

[3]Systems Engineering and Automation Department, University Carlos III of Madrid, Madrid, Spain

[4]Power Plant Monitoring and Control Research Department, Niroo Research Institute, Tehran, Iran

Correspondence
Vahab Haji Haji, Young Researchers and Elite Club, Borujerd Branch, Islamic Azad University, Borujerd, Iran.
Email: vhbhaji@gmail.com

Funding information
Spanish Ministry of Economy, Industry and Competitiveness, Grant/Award Number: DPI2016-75330-P

Abstract

This paper designs, implements, and compares the performance of a H_2, H_∞, H_2/H_∞, and *μ-synthesis* approach for a *V*94.2 gas turbine mounted in Damavand combined cycle power plant. The controllers are designed to maintain the speed and exhaust temperature within their desired intervals and to ensure the robust performance of the gas turbine power plant (GTPP) in the presence of uncertainties and load demand variations. A linear model of the GTPP is first estimated using V94.2 gas turbine real-time data and an autoregressive with exogenous input (ARX) identification approach, and then verified by residual analysis tests and steady-state performance. The H_2, H_∞, H_2/H_∞, and *μ-synthesis* controllers are then designed and implemented to the ARX model of the GTPP. The performance of the approaches is assessed and compared in terms of tracking capability, robustness, and transient performance. Additionally, the controllers' performance is compared to that of a conventional PID approach. Despite the slight variations in the performance, all the controllers exhibited robust stability and good overall performance in the presence of model uncertainties and load variations.

KEYWORDS

gas turbine power plant, H_2, H_2/H_∞, H_∞, robust control, *μ-synthesis*

1 | INTRODUCTION

Combined cycle power plants (CCPPs) are widely used in the electric power generation. They owe their popularity to their high efficiency, great flexibility, short installation time, and low installation cost.[1,2] In a CCPP, modeling, control, stability analysis, and reliability of a gas turbine unit are a challenging problem. This is due to the fact that the traditional PID-based controllers do not have proper performance due to parameter variations, unmodeled dynamics, modeling errors, modeling simplifications, or neglected nonlinearity, and may even result in system instability. Hence, robustness should be a major design feature when controlling a gas turbine power plant (GTPP).[1,3,4]

Various models have been proposed in the literature to accurately represent the dynamics of CCPP. A dynamic model for a single-shaft combined cycle plant including a supervisory control was proposed in.[3] The proposed model was assessed in terms of its stability and response to frequency transients during

*The research leading to these results has partially received funding from the HUMASOFT project (lead by author Concepción Alicia Monje), with reference DPI2016-75330-P, funded by the Spanish Ministry of Economy, Industry and Competitiveness.

full-load operations. A comparative study between different gas turbines and combined cycle models can be found in.[5,6] The authors of paper[5] compared the performance of a detailed model, GAST2A model, and GGOV1 model in terms of their responses regarding electric load and frequency transients. A verified combined cycle gas turbine model was considered in the study reported in.[2] The impact of combined cycle gas turbine dynamics on the frequency control of an island electricity system was also considered in that study. In,[4] Kakimoto et al investigated several combined cycle plants models to build a new one and then studied the dynamic behavior of the plant including temperature and speed control, fuel flow command, inlet guide vanes (IGV), and output power in the presence of frequency drops. The work reported in[7] focused on the frequency regulation issue and aimed at improving the combined cycle dynamic response and frequency regulation performance and maintaining the machine variables within a safe operational level. A combined cycle simple model for the investigation of abnormal frequency conditions can be found in.[8]

Likewise, various control approaches were proposed in the literature for the gas and steam turbines in a CCPP. Saikia et al[9] proposed a PID controller for the combined cycle gas turbine plant and used a firefly algorithm to optimize the controller gains. The performance and robustness of the proposed controller were investigated using the sensitivity analysis. A fractional-order fuzzy PID controller based on the particle swarm optimization algorithm was proposed for CCPP in the study by Haji-Haji and Monje.[1] The proposed controller was implemented in the speed control loop to improve the frequency response during any change in power demand or frequency deviation. Jadhav et al[10] took advantage of Bode's ideal loop transfer function to design a robust fractional-order controller for the speed loop to improve the frequency response of a gas turbine plant. In the study reported in,[11] a neuro-fuzzy--based controller was proposed and evaluated for set-point variations in a grid-connected heavy-duty gas turbine plant. Most of the above control approaches, however, lacked robustness to parameter variations and dynamic system mismatches. Gorbani et al[12] presented a model predictive controller (MPC) for a MS9001E gas turbine mounted in Montazer Ghaem Power Plant.

The performance of the GTPP is highly dependent upon the control strategy considered. Failure to provide proper control to any unwanted frequency drop or unit over temperature can negatively affect the power plant and finally lead to serious damage to the gas turbine components, and might even lead to system shutdown. Any frequency load fluctuation or set-point variation in power plants can cause instability in power grids and potentially lead to blackouts.

Furthermore, there are lots of discrepancies between the mathematical models (boiler, combustor, compressor, fuel system, air system, etc) used for design and the actual gas turbines' dynamics in practice. Therefore, designing robust controllers for such systems can have a great impact on their performance and life span. The proposed algorithms should not only be able to make the closed-loop power plant stable but also provide acceptable performance levels (tracking capability, transient and steady-state performance, etc) in the presence of frequency disturbance, unmodeled power plant dynamics, and measurement noise.

Due to the fact that robust control theory explicitly deals with uncertainty in its approach to control design, it has long been considered in controlling various systems.[13-15] In,[16] a H_∞ controller was designed for the speed and temperature control of a power plant gas turbine. It was shown that H_∞ resulted in improvements in the performance compared to MPC and PID controllers for the same conditions. *μ-synthesis* was considered in[17] to guarantee the robust stability (RS) and performance of an industrial hydraulic excavator. A multi-objective robust H_2/H_∞ fuzzy tracking approach was proposed in[18] to control the nonlinear superheat temperature system in a power plant.

In this study, we design, implement, and compare the performance of four robust control approaches for both temperature and speed control of a V94.2 gas turbine mounted in Damavand combined cycle plant. The proposed H_2, H_∞, H_2/H_∞, and *μ-synthesis* controllers aim at (a) guaranteeing the RS and performance of the closed-loop system in the presence of model uncertainties, (b) maintaining the temperature output within a desired level, and (c) improving the speed loop response for any frequency drop caused by a change in the power demand or output disturbances.

2 | NONLINEAR GAS TURBINE POWER PLANT MODEL

A simplified block diagram of a gas turbine plant including gas turbine, rotor inertia dynamics, fuel and air system, and temperature transducer is illustrated in Figure 1,[1] where air flow W_a and fuel flow W_f are the main manipulated signals, and rotor speed (frequency) N, power P_m, and exhaust temperature T_e are the main output signals. In Figure 1, the value of $T_{off} = 0.01$ (pu) refers to temperature offset; $K_W = 2.1281$ is the inverse of air control time constant; for the overheat control, 3.3 and 0.4699 are the time constant of overheat control and the overheat control integration rate, whereas 2.49 and 0.12 refer to the time constant of the speed control and the speed control integration rate, respectively. The description of other input/output signals used in Figure 1 is summarized in Table 1.

The speed and temperature control loops of the GTPP are shown in Figure 1. As Figure 1 shows (red line), the speed (frequency) control loop includes the speed controller, fuel limiter, fuel system, gas turbine dynamics, and rotor inertia. The main objective of the speed control loop is to act through minimum value selection and fuel system to compensate any difference between generation and load in the frequency deviation.

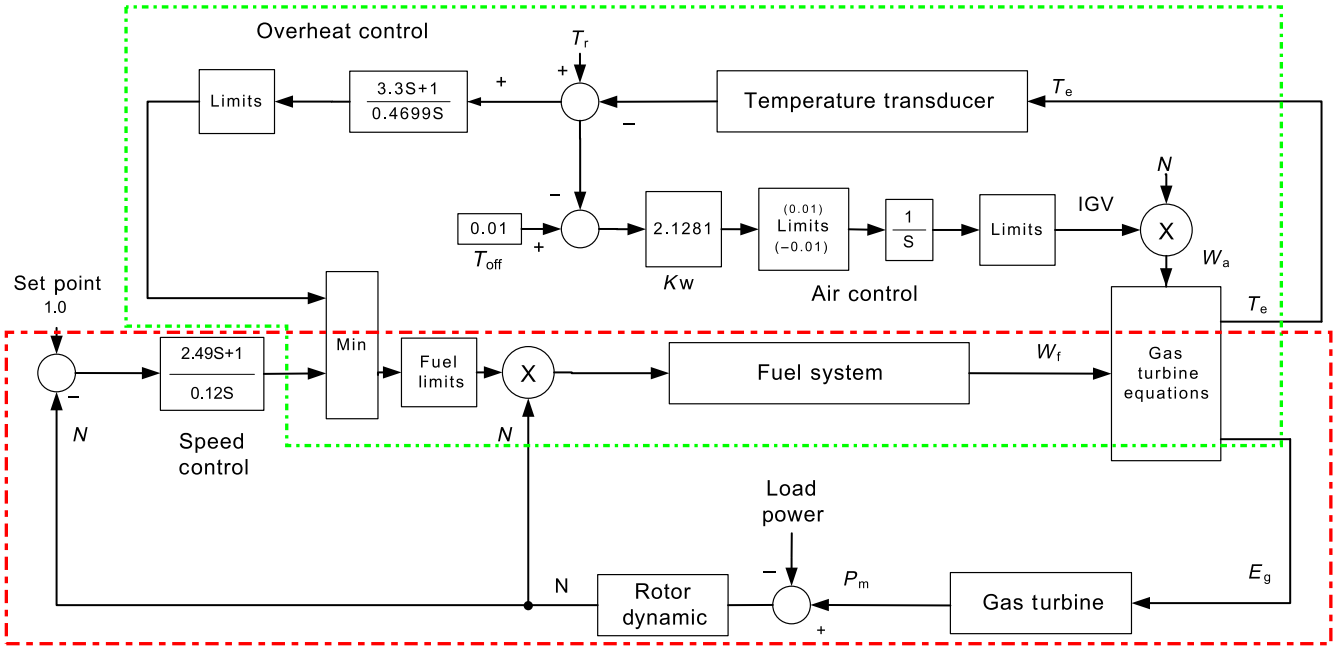

FIGURE 1 Simplified gas turbine plant model

The temperature control loop, on the other hand, includes the normal and overheat temperature control branches (Figure 1, green line). The main purpose of the overheat control branch is to reduce the fuel flow in order to prevent turbine overloading in extreme overheat cases. This loop includes fuel limits, fuel system, gas turbine dynamics, temperature transducer, and overheat controller. Note that, for a CCPP, a common practice in the industry consists on using the bottom steam cycle[19] when the exhaust temperature exceeds its limit. The normal temperature branch acts through the air system or IGV, and includes air control, gas turbine equations, and temperature transducer. This branch prevents the exhaust gas temperature from exceeding the reference value T_r. Note that the frequency (speed) and normal temperature loops are the main purpose of this paper; therefore, it is assumed that the overheat control temperature is not active all the time. Besides, there is an anti-windup mechanism included in temperature control loop to prevent the controller from saturation and to make sure that the controller can react properly to control GTPP. For a gas turbine process, the relationship between the inputs W_f and W_a and output T_f is[1,4]:

$$T_f = T_d + \left(T_{f0} - T_{d0}\right)\frac{W_f}{W_a}, \tag{1}$$

$$x = \left(Q_{r0} W_a\right)^{\frac{\gamma-1}{\gamma}}, \tag{2}$$

$$T_d = T_a\left(1 + \frac{x-1}{\eta_c}\right), \tag{3}$$

where T_{f0} is the rated value for the gas turbine inlet temperature, T_{d0} is the rated value for the compressor discharge temperature, x is the compressor temperature ratio, P_{r0} is the nominal compressor pressure ratio, γ is the ratio of specific heats, and η_c represents the compressor efficiency. The gas turbine inlet temperature T_f can be expressed as follows:

$$T_e = T_f\left[1 - \left(1 - \frac{1}{x}\right)\eta_t\right], \tag{4}$$

where η_t is the turbine efficiency. The energy supplied to gas turbine is given by:

$$E_g = K_0\left\{\left(T_f - T_e\right) - \left(T_d - T_a\right)\right\} W_a, \tag{5}$$

where K_0 is the gas turbine coefficient. Further details about the parameters and specifications of the GTPP model can be found in.[1,3,4]

3 | GAS TURBINE POWER PLANT SYSTEM IDENTIFICATION AND VALIDATION

According to the ARX structure, the relationship between the estimated output $y(t)$, measured data input $u(t)$, and white-noise disturbance value $e(t)$ can be described as[20]:

$$\begin{aligned} &y(t) + a_1 y(t-1) + \cdots + a_{na} y(t-na) = \\ &b_1 u(t-nk) + \cdots + b_{nb} u(t-nb-nk+1) + e(t), \end{aligned} \tag{6}$$

TABLE 1 Main input/output signals of the GTPP model

Signals	Definition
P_m	Gas turbine generated power (pu)
E_g	Thermal power converted by the gas turbine
T_e	Exhaust temperature (pu)
T_r	Reference temperature (pu)
T_a	Ambient temperature (°C)
T_f	Gas turbine inlet temperature (pu)
F_d	Fuel demand signal (pu)
N	Rotor speed (frequency)
W_a	Air flow
W_f	Fuel flow (pu)
IGV	Inlet guide vanes
T_{f0}	Rated value for gas turbine inlet temperature (°C)
T_{d0}	Rated value for the compressor discharge temperature (°C)
x	Compressor temperature ratio
η_t	Turbine efficiency

where $u(t-\text{nk})$ and $y(t-\text{na})$ refer to the past inputs and outputs, respectively, na is the number of poles, nb is the number of zeroes plus 1, and nk is the dead time. Then, a and b are constant factors that could be estimated using the least square error method (LSM).

As Figure 1 shows, the airflow W_a is obtained by multiplying N by IGV. This means that any change in IGV can not only affect the exhaust temperature but also impact the power and frequency outputs. Thus, the IGV signal needs to be considered as an input in the estimation process. According to Figure 1, in order to estimate a linear ARX model for the speed loop, the fuel flow Fuel, output frequency N, ambient temperature T_a, and IGV should be considered as input variables, whereas the power demand P_m should be considered as output signal. The equation relating the frequency (speed) output N with the inputs Fuel, T_a, and IGV can be determined using the rotor dynamics and P_m. Note also that the input signal Fuel is equal to fuel demand signal (Fd) for a power plant under normal operating conditions.

Similarly, based on Figure 1 for the temperature loop, the variables Fuel, N, T_a, and IGV are considered as inputs, and the exhaust temperature T_e as output. In this paper, the considered base load for the V94.2 GTPP is 115MW and the atmospheric pressure is around 896.5 (mbar). The modeling and identification has been done around V94.2 gas turbine operating point. T_a is 30°C or 303 K, IGV is [0.52, 1], N is [0.95, 1], and Fuel is [0, 1.0]. Figure 2 shows the real data for V94.2 gas turbine in Damavand CCPP. The data are collected from no-load to full-load conditions with sampling time equals to 1 seconds. Note that, in the case of control loops, the main focus is on frequency and normal temperature loops; hence, the overheat control loop is not active during the simulation process and the Fuel signal is equal to F_d.

The identified block diagram of the gas turbine plant CP(s) is shown in Figure 3, where P_d represents the demand power (per unit (pu)). Based on Equation 6 and the ARX structure, the transfer functions presented in Figure 3 are as follows:

$$G_1(s)=\frac{P_m(s)}{\text{Fuel}(s)}=\frac{0.65s^3+0.46s^2+0.569s+0.0412}{s^4+0.988s^3+2.208s^2+0.645s+0.033}, \quad (7)$$

$$G_2(s)=\frac{P_m(s)}{N(s)}=\frac{-2.121s^3-2.896s^2-1.94s-0.017}{s^4+0.988s^3+2.208s^2+0.645s+0.033}, \quad (8)$$

$$G_4(s)=\frac{P_m(s)}{T_a(s)}=\frac{-0.008s^3+0.001s^2-0.003s+2.756\times10^{-05}}{s^4+0.988s^3+2.208s^2+0.645s+0.033}, \quad (9)$$

$$G_5(s)=\frac{P_m(s)}{\text{IGV}(s)}=\frac{0.061s^3+0.071s^2+0.115s+0.00071}{s^4+0.988s^3+2.208s^2+0.645s+0.033}, \quad (10)$$

$$G_6(s)=\frac{T_e(s)}{N(s)}=\frac{13.22s+0.050}{s^2+6.31s+0.096}, \quad (11)$$

$$G_7(s)=\frac{T_e(s)}{T_a(s)}=\frac{-0.025s-5.32\times10^{-05}}{s^2+6.31s+0.096}, \quad (12)$$

$$G_8(s)=\frac{T_e(s)}{\text{Fuel}(s)}=\frac{1.45s+0.094}{s^2+6.31s+0.096}, \quad (13)$$

$$G_9(s)=\frac{T_e(s)}{\text{IGV}(s)}=\frac{-1.34s-0.028}{s^2+6.31s+0.096}, \quad (14)$$

In Figure 3, $G3$ (s) represents the rotor dynamics, which can be estimated as:

$$G_3(s)=\frac{1}{14.5s}. \quad (15)$$

In a time series format, the transfer functions are as follows:

$$G_1=(0.198\mp0.005i)e^{t(-0.334\pm1.36i)}+0.0157e^{-0.0661t}+0.239e^{-0.255t}, \quad (16)$$

$$G_2=(-0.737\pm0.552i)e^{t(-0.334\pm1.36i)}+0.272e^{-0.0661t}-0.92e^{-0.255t}, \quad (17)$$

$$G_3=0.069, \quad (18)$$

$$G_4=(-0.003\mp0.002i)e^{t(-0.334\pm1.36i)}+0.0007e^{-0.0661t}-0.003e^{-0.255t}, \quad (19)$$

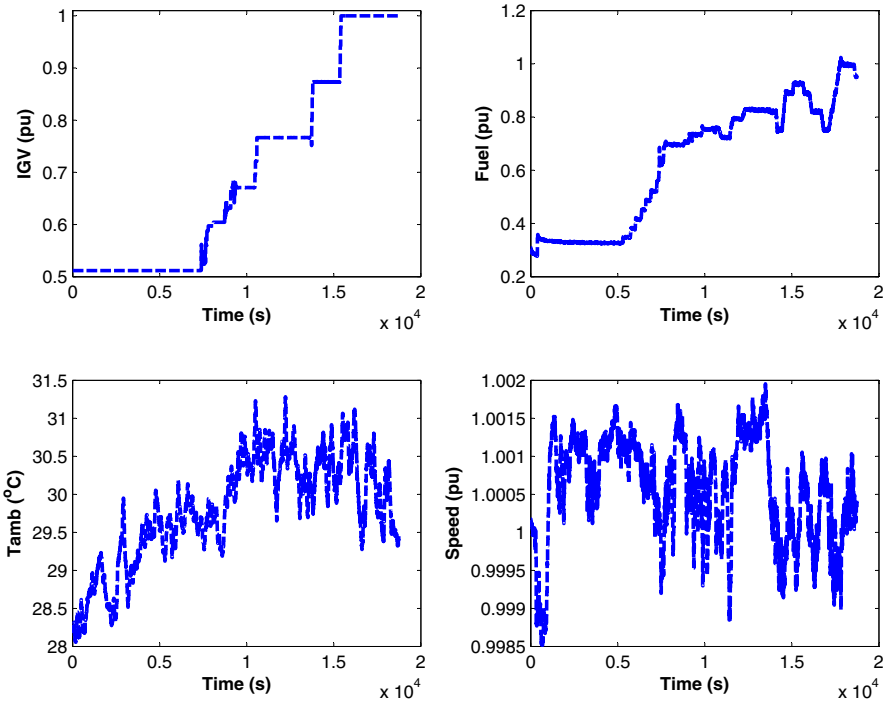

FIGURE 2 Measured signals for the V94.2 gas turbine power plant

$$G_5 = (0.004 \mp 0.0111i)e^{t(-0.334 \pm 1.36i)} - 0.0181e^{-0.0661t} + 0.071e^{-0.255t}, \tag{20}$$

$$G_6 = 13.2e^{-3.16t}(\cosh(3.14t) - 1.0\sinh(3.14t)), \tag{21}$$

$$G_7 = -0.0247e^{-3.16t}(\cosh(3.14t) - 1.0\sinh(3.14t)), \tag{22}$$

$$G_8 = 1.45e - 3.16t\,(\cosh(3.14t) - 0.984\sinh(3.14t)), \tag{23}$$

$$G_9 = -1.34e^{-3.16t}(\cosh(3.14t) - 0.998\sinh(3.14t)). \tag{24}$$

Figure 4 provides the steady-state diagram for the identified ARX model, where the power plant variables T_e, IGV, and Fuel are plotted versus changes in the power demand (pu). Two operating regions can be distinguished in Figure 4. In the first (I) operating region, the temperature T_e is lower than the set point; therefore, IGV is set to its minimum value (0.52 (pu)). When increasing the fuel flow, the exhaust temperature rises to the reference (Tr = 1) and the power demand to 0.7917, and then, the power plant enters the operating region II. In this region, the temperature control loop acts via the IGV control to maintain T_e at its reference value.

The estimated linear model specifications and measured and simulated model outputs for the speed and temperature loops are illustrated in Table 2 and Figure 5, where MSE refers to the mean square normalized error performance function, FPE is Akaike's final prediction error, and Fit is fitness percentage. As Figure 5 shows, the simulated outputs closely follow GTPP power and temperature outputs. Based on the residual analysis tests, and measured and simulated model outputs, it was found that the estimated linear ARX model is accurate enough to describe the behavior of the gas turbine plant. This can also be verified by the fitness results illustrated in Table 2, which are 94.7% for the temperature loop and 92.72% for speed loop. Additional assessment of the identified model including the speed CP_{Speed} and temperature CP_{Temp} loops will be performed in Simulation section.

4 | ROBUST CONTROL FORMULATION

The standard block diagram of the robust control method including external inputs w, control inputs u, output signals z, and measured outputs y is presented in Figure 6. In this figure, M(s) and $K(s)$ refer to the plant model and controller, respectively. The main control objective is to find a controller $K(s)$ that would stabilize plant M(s) and minimize a norm of the transfer function from input w to output z. In this paper, the objective function that would maintain the turbine speed and the exhaust temperature within their desired interval is S/KS, with S the sensitivity function and K the controller function.

Note that, according to Figure 1, the overheat control branch only acts in the extreme overheat cases to prevent

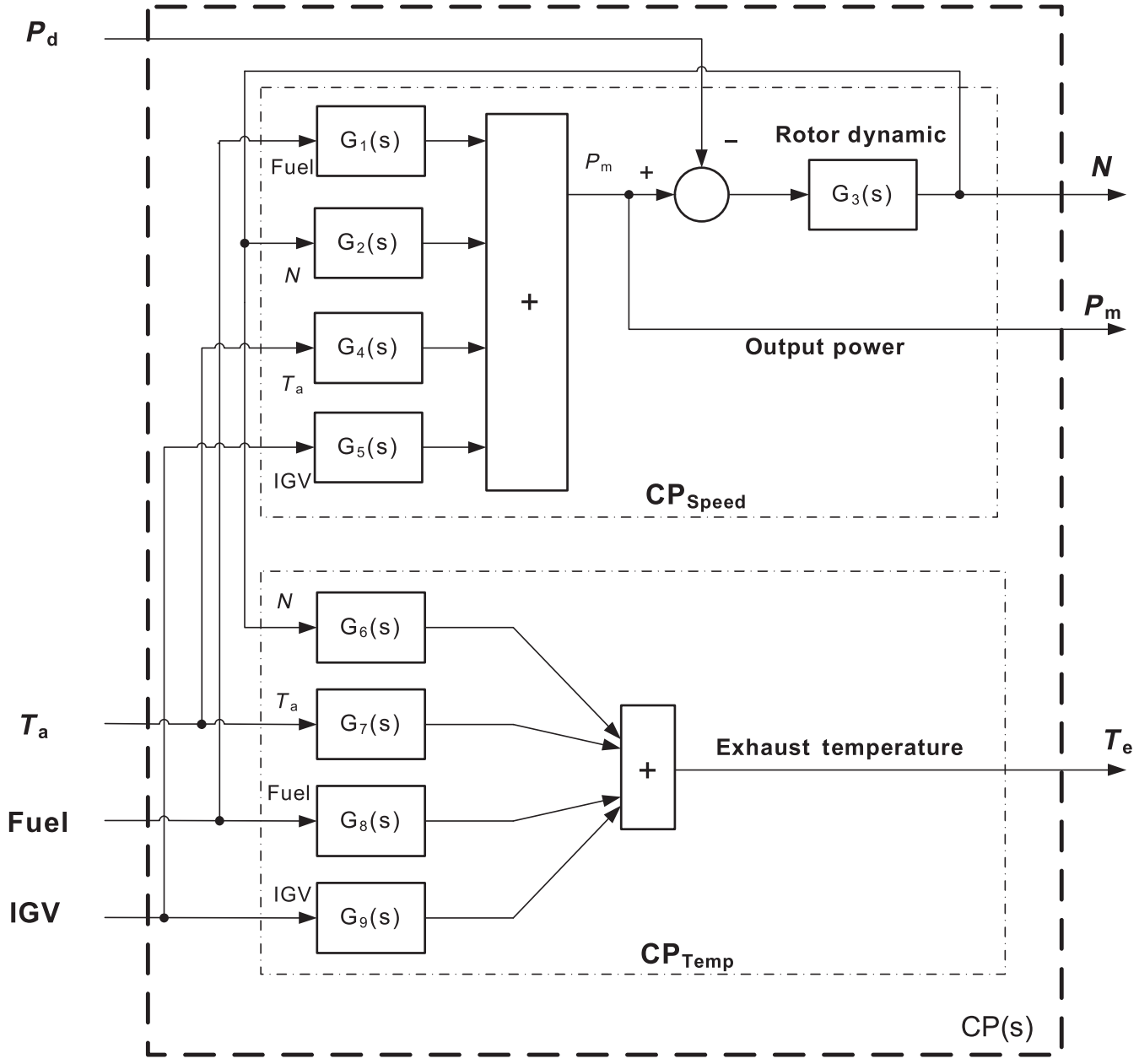

FIGURE 3 Block diagram of the power plant linear model

turbine overloading. Thus, this control branch is not active during the normal operation and there is no direct feedback from the output temperature error e_T to the speed controller. Note also that, based on Equation 5, the output power can be affected by the air flow or IGV control, and this impact can be considered as an input disturbance in the robust control design procedure. Similarly, according to Figure 1 (green line) for temperature control loop, there is no direct feedback from the output speed error e_N to the temperature controller. Thus, the speed and temperature loops could either be controlled using a multi-inputs, multi-outputs (MIMO) controller or two single-input, single-output (SISO) controllers.

Figures 7 and 8 represent the linear estimated model of the speed and temperature loops of the GTPP, where Fuel and IGV are the manipulated variables, whereas N and T_e are the measured outputs. N_{ref}, P_d, T_{ref}, and T_a are the reference inputs, and Z_N, Z_{Temp}, Z_{Fuel}, and Z_{IGV} are the weighted output signals. Two variables e_N and e_T are used to show the error of the speed and temperature loops, respectively. Here, the speed error is defined as the difference between speed reference N_{ref} and the actual speed N. Similarly, the temperature error is computed using the difference between temperature reference T_{ref} and the actual temperature T_e. Besides, W_N, W_{Temp}, W_{Fuel}, and W_{IGV} refer to the speed, temperature, fuel,

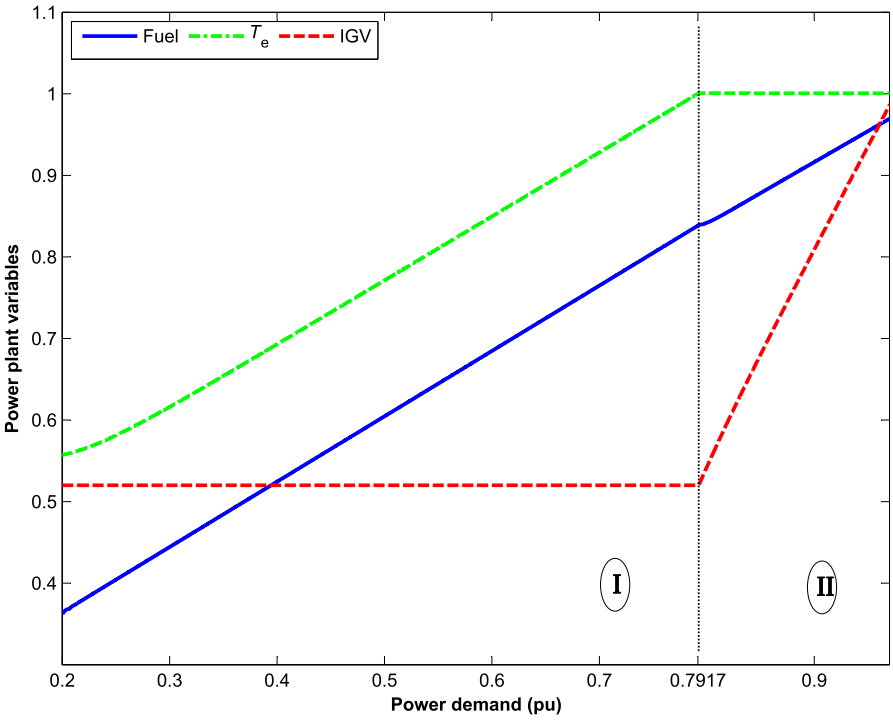

FIGURE 4 Steady-state diagram for GTPP and estimated model

and IGV weighting functions, respectively. M_{Speed} and M_{Temp} refer to the weighted transfer functions for the speed and temperature loops, respectively. In this paper, for the sake of simplicity, we will design two SISO robust controllers for the combined cycle plant.

According to Figures 6 and 7, the relationship between the inputs $w(s)$ and $u(s)$ and the outputs $z(s)$ and $y(s)$ can be defined by:

$$\begin{bmatrix} z(s) \\ y(s) \end{bmatrix} = M_{\text{Speed}}(s) \begin{bmatrix} w(s) \\ u(s) \end{bmatrix}, \tag{25}$$

where w, u, z, y, and M_{Speed} can be defined as follows:

$$w = \begin{bmatrix} N_{\text{ref}} \\ P_{\text{d}} \\ T_{\text{a}} \\ \text{IGV} \end{bmatrix}, \quad u = \text{Fuel}, \quad z = \begin{bmatrix} Z_N \\ Z_{\text{Fuel}} \end{bmatrix}, \quad y = e_{\text{N}}, \tag{26}$$

$$M_{\text{Speed}} = \begin{bmatrix} M_{11}(s) & M_{12}(s) \\ M_{21}(s) & M_{22}(s) \end{bmatrix} \tag{27}$$

where

$$\begin{aligned} M_{21}(s) &= \begin{bmatrix} 1 & \frac{G_3}{1-G_2G_3} & \frac{-G_4G_3}{1-G_2G_3} & \frac{-G_5G_3}{1-G_2G_3} \end{bmatrix}, \\ M_{22}(s) &= \begin{bmatrix} \frac{-G_1G_3}{1-G_2G_3} \end{bmatrix}, \quad M_{11}(s) = \begin{bmatrix} W_N M_{21} \\ 0_{1*4} \end{bmatrix}, \\ M_{12}(s) &= \begin{bmatrix} W_N M_{22} \\ W_{\text{Fuel}} \end{bmatrix}. \end{aligned} \tag{28}$$

TABLE 2 ARX model specifications and characteristics

	MSE	FPE	Fit %
T_{e}	1.161×10^{-05}	1.179×10^{-05}	94.7
P_{m}	1.917×10^{-04}	1.927×10^{-04}	92.72

The transfer function (T_{zw}) from w to z can be written as follows:

$$F_l(M_{\text{Speed}}, K_{\text{Speed}}) = M_{11} + M_{12}K_{\text{Speed}}(I - M_{22}K_{\text{Speed}})^{-1}M_{21}. \tag{29}$$

Similarly, for temperature control loop and from Figures 6 and 8, the relationship between inputs $w(s)'$ and $u(s)'$ and outputs $z(s)'$ and $y(s)'$ can be described by:

$$\begin{bmatrix} z(s)' \\ y(s)' \end{bmatrix} = M_{\text{Temp}}(s) \begin{bmatrix} w(s)' \\ u(s)' \end{bmatrix}, \tag{30}$$

where w', u', z', y', and M_{Temp} are:

$$w' = \begin{bmatrix} T_{\text{ref}} \\ N \\ T_{\text{a}} \\ \text{Fuel} \end{bmatrix}, \quad u' = \text{IGV}, \quad z' = \begin{bmatrix} Z_{\text{Temp}} \\ Z_{\text{IGV}} \end{bmatrix}, \quad y' = e_T, \tag{31}$$

$$M_{\text{Temp}}(s) = \begin{bmatrix} M'_{11}(s) & M'_{12}(s) \\ M'_{21}(s) & M'_{22}(s) \end{bmatrix}, \tag{32}$$

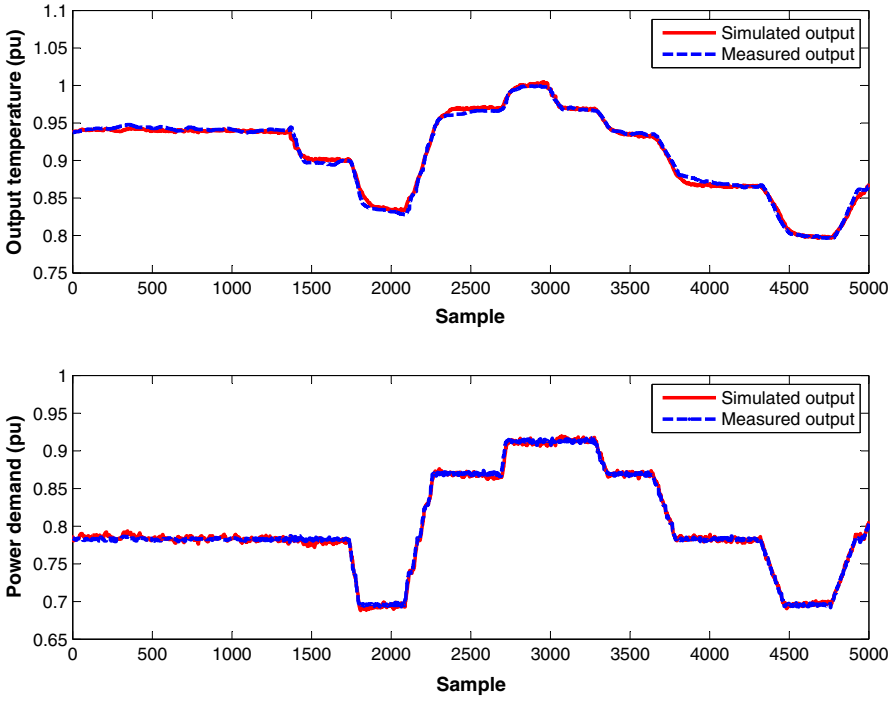

FIGURE 5 Measured and simulated model outputs for the temperature and speed loops

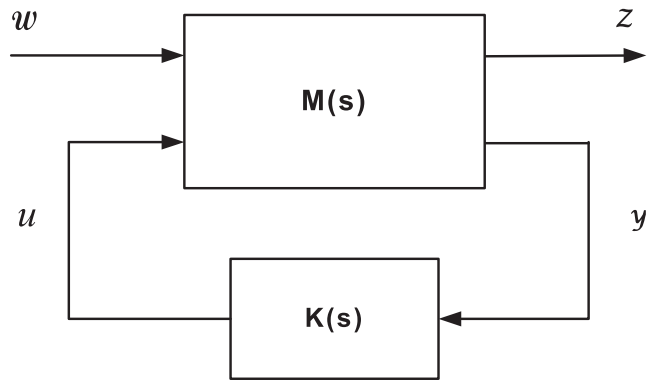

FIGURE 6 Robust control block diagram

where

$$M'_{21}(s)=\begin{bmatrix} 1 & -G_6 & -G_7 & -G_8 \end{bmatrix},$$
$$M'_{22}(s)=-G_9,$$
$$M'_{11}(s)=\begin{bmatrix} W_{\mathrm{IGV}}M'_{21} \\ 0_{1*4} \end{bmatrix},\quad M'_{12}(s)=\begin{bmatrix} W_{\mathrm{Temp}}M'_{22} \\ W_{\mathrm{IGV}} \end{bmatrix}. \tag{33}$$

In Equation 31, N is equal to N_{ref}, and the transfer function (T'_{zw}) from w' to z' for the temperature control loop is defined by:

$$F'_1(M'_{\mathrm{Temp}},K_{\mathrm{Temp}})=M'_{11}+M'_{12}K_{\mathrm{Temp}}(I-M'_{22}K_{\mathrm{Temp}})^{-1}M'_{21}. \tag{34}$$

For the frequency (speed) control loop (Figure 7 and Equation 26), the manipulated variable is fuel flow (Fuel) and the controlled variable is output frequency (N), whereas N_{ref}, P_{d}, T_{a}, and IGV represent the reference and disturbance inputs. For the temperature control loop (Figure 8 and Equation 31), the manipulated variable is IGV and the controlled variable is exhausted temperature T_{e}, whereas T_{ref}, N, T_{a}, and Fuel represent the reference and disturbance inputs.

4.1 | H_2 control strategy

The main purpose of considering an H_2 design for the speed and temperature control of GTPP is to find a controller $K(s)$ that would (a) internally stabilize M(s) and (b) minimize the second norm of the following transfer function, where W_1 and W_2 are the weighting functions[21,22]:

$$\min_{K\ \text{stabilizing}} \left\| \begin{matrix} W_1(I+MK)^{-1} \\ W_2K(I+MK)^{-1} \end{matrix} \right\|_2. \tag{35}$$

For the speed loop in the combined cycle plant model, Equation 35 can be rewritten as follows:

$$\min_{K_{\mathrm{Speed}}\ \text{stabilizing}} \left\| \begin{matrix} W_N(I+M_{\mathrm{Speed}}K_{\mathrm{Speed}})^{-1} \\ W_{\mathrm{Fuel}}K(I+M_{\mathrm{Speed}}K_{\mathrm{Speed}})^{-1} \end{matrix} \right\|_2. \tag{36}$$

And for the temperature control loop, we have the following:

$$\min_{K_{\mathrm{Temp}}\ \text{stabilizing}} \left\| \begin{matrix} W_{\mathrm{Temp}}(I+M_{\mathrm{Temp}}K_{\mathrm{Temp}})^{-1} \\ W_{\mathrm{IGV}}K(I+M_{\mathrm{Temp}}K_{\mathrm{Temp}})^{-1} \end{matrix} \right\|_2. \tag{37}$$

For this H_2 optimization problem, the weighting functions are as follows:

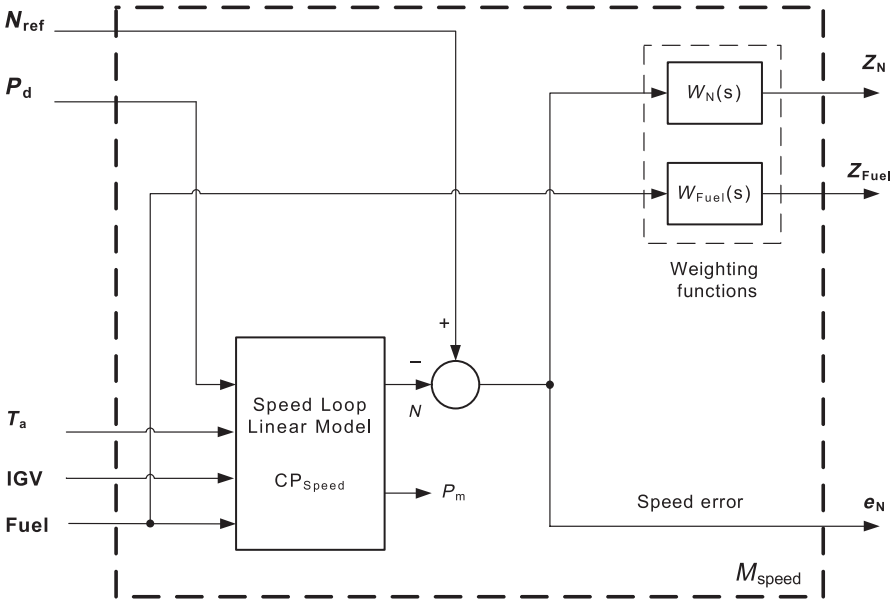

FIGURE 7 The speed loop linear model with weighting functions and reference signals

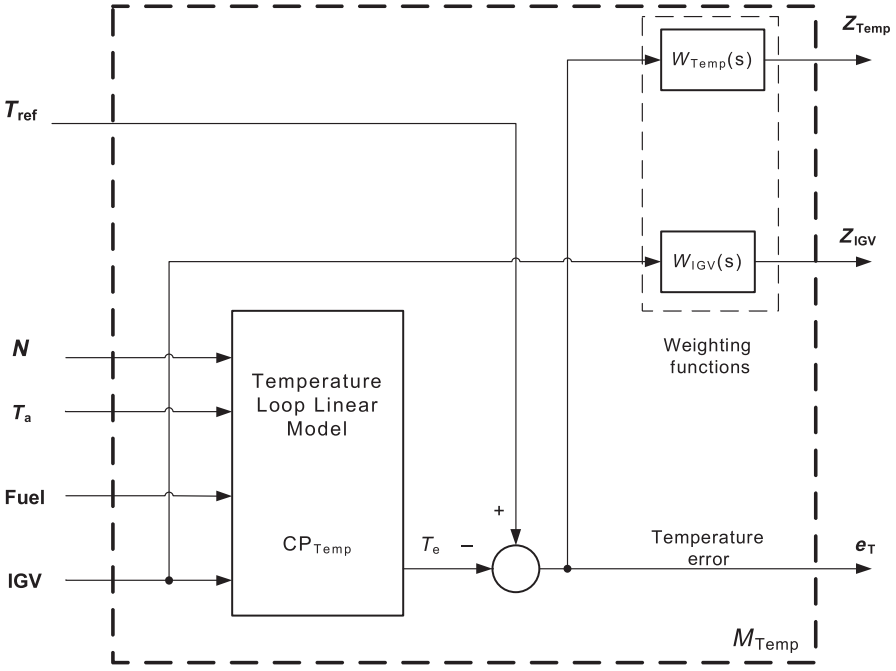

FIGURE 8 The temperature loop linear model with weighting functions and reference signals

$$W_N = \frac{s+9.054}{30.18s+0.00097}, \quad W_{\text{Fuel}} = 0.02,$$
$$W_{\text{Temp}} = \frac{s+2}{20s+0.006}, \quad W_{\text{IGV}} = 0.01. \tag{38}$$

4.2 | H_∞ control strategy

Similarly, the main goal of using H_∞ for the speed and temperature loops of the power plant is to find a controller $K(s)$ to internally stabilize $M(s)$ and, at the same time, to minimize the infinite norm of Equations 36 and 37.[23] By choosing appropriate weighting functions, H_∞ can provide RS and nominal performance of the final closed-loop system. In this H_∞ problem, the weighting functions are as follows:

$$W_{\text{N}} = \frac{s+9.054}{30.18s+0.00097}, \quad W_{\text{Fuel}} = 0.02,$$
$$W_{\text{Temp}} = \frac{s+2}{20s+0.006}, \quad W_{\text{IGV}} = 0.01. \tag{39}$$

4.3 | H_2/H_∞ control strategy

Mixed H_2/H_∞, control combines the disturbance rejection properties of H_∞ design with the ability of H_2 to improve the transient behavior of the system against random disturbances.[24,25] In this paper, the weighting functions for the

H_2/H_∞ controller and power plant optimization problem are as follows:

$$W_{\mathrm{N}}^{h_\infty}=\frac{s+9.054}{30.18s+0.00097},\quad W_{\mathrm{Fuel}}^{h_\infty}=0.01,\quad W_{\mathrm{Fuel}}^{h_2}=0.015,$$
$$W_{\mathrm{Temp}}^{h_\infty}=\frac{s+8}{20s+0.016},\quad W_{\mathrm{IGV}}^{h_\infty}=0.01,\quad W_{\mathrm{IGV}}^{h_2}=0.01. \tag{40}$$

In Equation 40, the superscripts h_∞ and h_2 refer to the weighting functions for H_∞ and H_2 problems, respectively.

4.4 | *μ-synthesis* control strategy

Compared to H_∞, the *μ-synthesis* method based on the singular value μ and *D–K* iteration procedure can be proposed to ensure the RS and performance of the closed-loop system.[26] In the *μ-synthesis* strategy, the aim is to find the controller K that would minimize the following optimization problem[26,27]:

$$\min_{K}\ \inf_{D,D^{-1}\in H_\infty}\left\|DF_{\mathrm{l}}(M,K)D^{-1}\right\|_\infty. \tag{41}$$

For the GTPP speed loop, the above equation can be rewritten as follows:

$$\min_{K_{\mathrm{Speed}}}\ \inf_{D,D^{-1}\in H_\infty}\left\|DF_{\mathrm{l}}(M_{\mathrm{Speed}},K_{\mathrm{Speed}})D^{-1}\right\|_\infty. \tag{42}$$

Similarly, for the temperature loop we have the following:

$$\min_{K_{\mathrm{Temp}}}\ \inf_{D,D^{-1}\in H_\infty}\left\|DF_{\mathrm{l}}(M_{\mathrm{Temp}},K_{\mathrm{Temp}})D^{-1}\right\|_\infty. \tag{43}$$

In Equations 41-43, $K(s)$ and $D(k)$ can be achieved by the *D–K* iteration procedure. The weighting functions are as follows:

$$W_N=\frac{s+0.73}{24.18s+0.00007},\quad W_{\mathrm{Fuel}}=0.01,$$
$$W_{\mathrm{Temp}}=\frac{s+0.6}{20s+0.0007},\quad W_{\mathrm{IGV}}=0.001. \tag{44}$$

All weighting functions are selected based on the IGV, temperature, frequency, and power limitations in order to provide the best transient and steady-state behavior in terms of tracking capability and disturbance rejection. For the speed control loop, the main purpose is to maintain the output frequency near to 50 Hz and to avoid from oscillations as much as possible. In the case of temperature loop, the aim is to maintain the output temperature T_{c} lower than Tr = 539°C.

5 | SIMULATION RESULTS AND COMPARISON ANALYSIS

In this section, after analyzing the accuracy of the ARX linear model, we assess the performance of the robust controllers and compare their performance in terms of tracking capability, robustness, and transient behavior.

In order to design the H_2, H_∞, H_2/H_∞, and *μ-synthesis* robust controllers for the GTPP, model uncertainties (up to 5%) are first included into the estimated transfer functions in Equations 7-15. These latter are then combined with Equations 38-40 and 44 for weighting functions and used to calculate Equations 25-28 for the speed control loop and Equations 30-33 for the temperature control loop. Finally, the H_2, H_∞, H_2/H_∞, and *μ-synthesis* methods described in Robust control formulation section are considered to compute the best controller $K(s)$ that would stabilize $M_{\mathrm{Speed}}(s)$ in Equation 27 and $M_{\mathrm{Temp}}(s)$ in Equation 32, and that would also minimize the mixed sensitivity cost function presented in Equations 36 and 37 for the temperature and speed control loops, respectively.

Figure 9 shows the RS and robust performance (RP) of all four approaches. The lower bounds of the singular values μ for speed and temperature loops are shown in Table 3. According to Figure 9 and Table 3, all four controllers H_2, H_∞, H_2/H_∞, and *μ-synthesis* can provide the RS and performance of the closed-loop gas turbine plant. From Figure 9 and Table 3, for the speed control loop, the H_∞ and μ controllers provide the best RS and RP, respectively, while this latter is achieved by H_∞ controller for the temperature loop.

The frequency responses of the speed and temperature closed loops are shown in Figures 10 and 11, respectively. Note that H_∞ and *μ-synthesis* display larger bandwidths compared to the rest of the controllers. Although this property offers a better transient response for the speed and temperature loops, it can result in further noise amplification. As shown in Figure 11, all the controllers are characterized by low gains in high-frequency ranges to deal with unmodeled dynamics, whereas in low-frequency ranges, high gains are required to reduce steady-state tracking errors and properly attenuate disturbances.

The GTPP model uncertainty is increased from 0 to 1 (0% to 100%), and the simulation results are provided in Figures 12 and 13 and Table 4. In these figures and table, the maximum gain (Max-Gain), stability margin (Stab-Margin), and performance margin (Perf-Margin) are plotted versus changes in the model uncertainty, and Stab-Uncer and Perf-Uncer refer to the uncertainty points where the stability and performance curves go below 1. From the figures, it is clear that these two last uncertainty numbers are equal to the points where the gain curve goes above 1 and to infinity, respectively. To understand the data provided in the figures and table, the explanation of three aspects is necessary: (a) The maximum gain is the possible largest value for the closed-loop Bode diagram over an uncertainty range, and it is in a close connection with stability and performance margins, where a bigger gain leads to a lower margin. Two numbers are indicated in Table 4

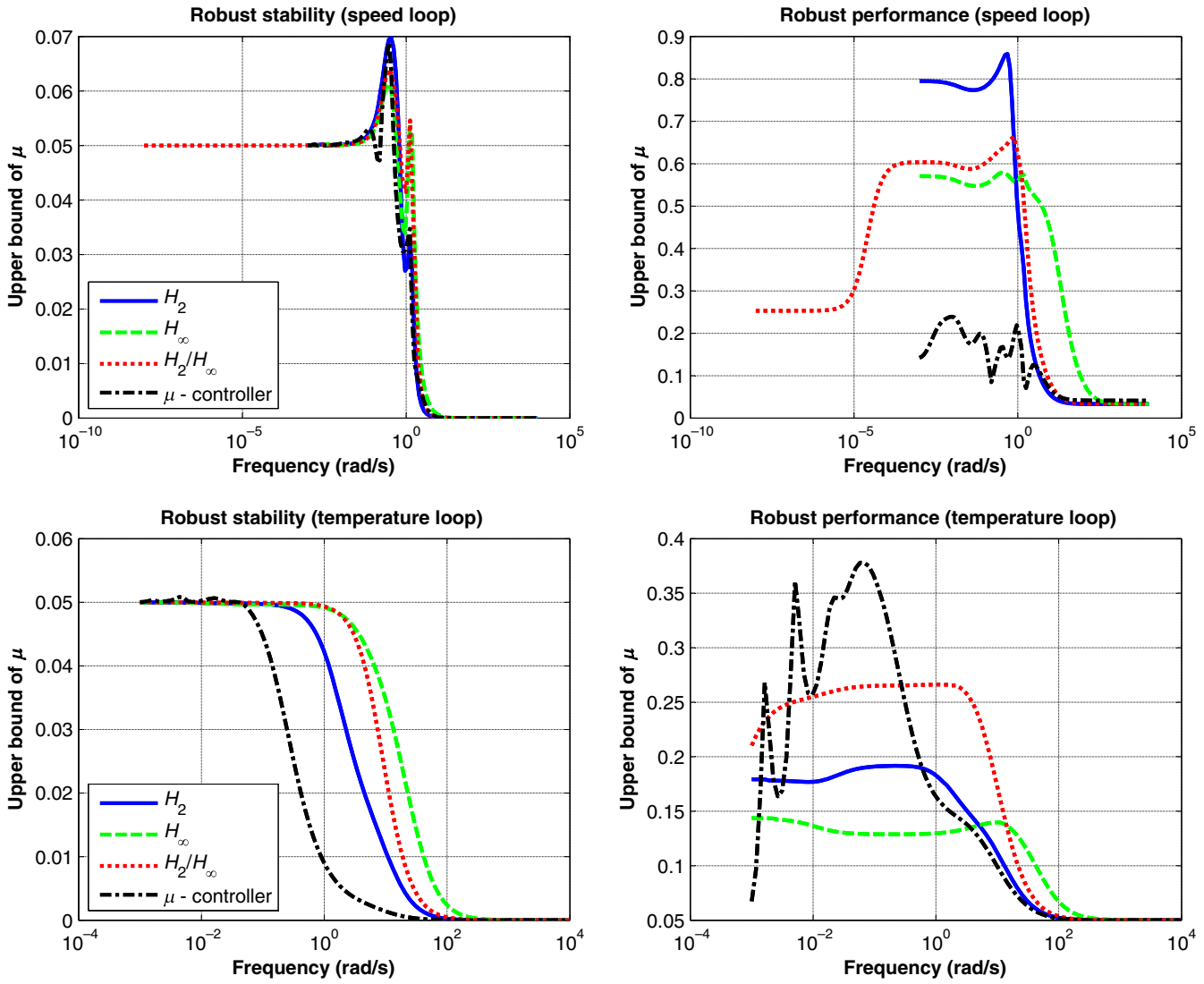

FIGURE 9 Closed-loop robust stability and robust performance

for maximum gain: The first one is for 5% uncertainty for speed and temperature loops, and the second one is for maximum uncertainty just before the gain goes to infinity; (b) in Table 4, the stability margin refers to the point of the stability curve in Figures 12 and 13 where the uncertainty is 5% for speed and temperature loops; (c) similarly, the performance margin is the point where performance curves in Figures 12 and 13 cross the uncertainty 5% for speed and temperature loops.

As Figure 12 and Table 4 show, in the case of speed loop, the *μ-synthesis* robust controller provides the best maximum gain (0.18 for 5% uncertainty) and performance margin (4.9) compared to the other robust controllers. Similarly, the H_∞ controller presents the best stability margin (16.52). These results are in close connection with the uncertainties of 0.79 and 0.65 (Table 4) for H_∞ and *μ-synthesis*, respectively, where a bigger GTPP model uncertainty (Stab-Uncer and Perf-Uncer) yields better performance and stability margins. A big frequency gain (1.0) for H_2 controller leads to worse stability and performance margins. As for temperature control loop, based on Figure 13 and Table 4, the H_2 robust controller presents the best gain and stability margins, while the best performance margin result is for H_∞ controller. The *μ-synthesis* robust controller provides the worst performance margin. This can also be corroborated by the results in Figure 13.

In order to assess and compare the performance of the different controllers in terms of tracking capability, robustness, and transient performance, two simulation scenarios illustrating (a) tracking and (b) disturbance rejection are considered:

- In the tracking scenario, the speed reference N_{ref} is initially set to 1; $T_{\text{ref}} = 1$ pu; after 1450*s*, demand load P_{d} changes from 0.65 to 0.78 pu, and after 650*s*, it decreases to 0.68 pu. Here, the goal is to evaluate the transient and steady-state responses of the gas turbine plant for changes in the power demand. The transient response of the GTPP is illustrated

in Figure 14 for all four controllers. The results are also compared to those from the PID-based controller, where PID refers to the PI (speed control block) and *I* (air control block) controllers for the speed and temperature loops in Figure 1. The proportional and integral coefficients of the PI and *I* controllers are based on the procedure provided in[4] and.[28] The optimum time indices (maximum overshoot M_P, rise time T_r and settling time T_s) and output errors of integral time absolute error (ITAE), integral absolute error (IAE), integral time squared error (ITSE), and integral squared error (ISE)[29] for all the control strategies are summarized in Tables 5 and 6, respectively.

- In the disturbance rejection scenario, the transient response of the GTPP is evaluated for a 1% instantaneous frequency drop, where the power and temperature references are fixed to 0.76 and 1 pu, respectively. Figure 15 and Table 7 show the output responses of the GTPP for ISE, IAE, ITSE, ITAE, mean, standard deviation, and maximum deviation of output errors for this frequency disturbance.

The results from Figures 14 and 15 and Tables 3, 4, 5, 6 and 7 clearly show that the behavior of the closed-loop system is in close connection with the selected weighting functions in Equations 38-40 and 44 and the design specifications. In the gas turbine plant model, the fuel system has a direct effect on the speed and temperature control loops. As Figures 14 and 15 show, any change in fuel command results in changes in the temperature, power, and speed outputs. Furthermore, any unwanted drop or change in the frequency output due to the presence of an inappropriate speed control can negatively affect the power plant and potentially damage the gas turbine components, and even lead to a system shutdown. Note that

TABLE 3 Robust stability (RS) and robust performance (RP) lower bounds for speed (*S*) and temperature (*T*) loops

Controller	RS(*S*)	RP(*S*)	RS(*T*)	RP(*T*)
H_2	14.34	1.16	**20.01**	5.22
H_∞	**16.30**	1.73	**20.00**	**6.95**
H_2/H_∞	15.61	1.51	**20.00**	3.76
μ	14.49	**4.18**	19.68	2.65

The bold values are the best simulation results.

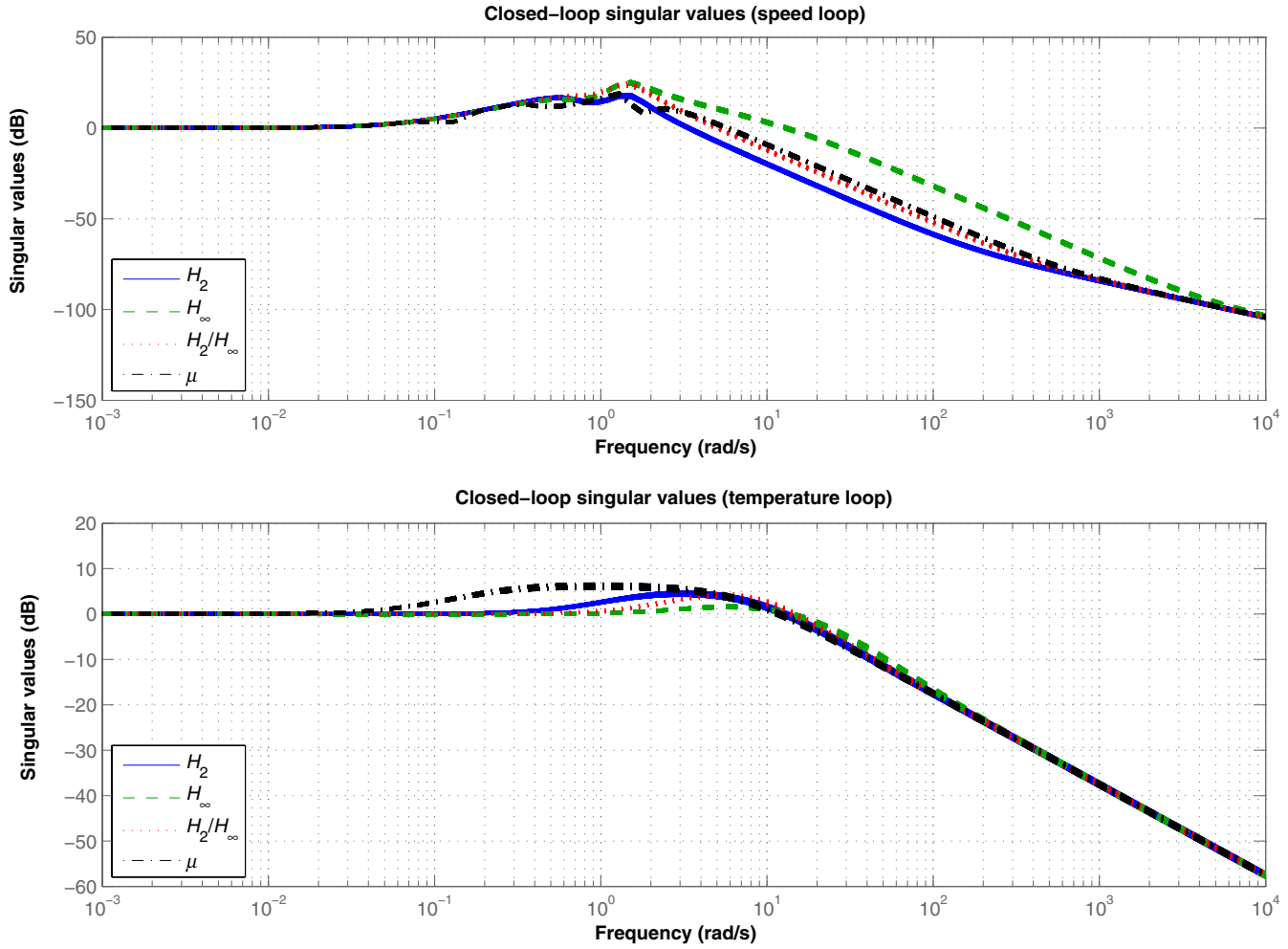

FIGURE 10 Speed and temperature closed-loop frequency responses

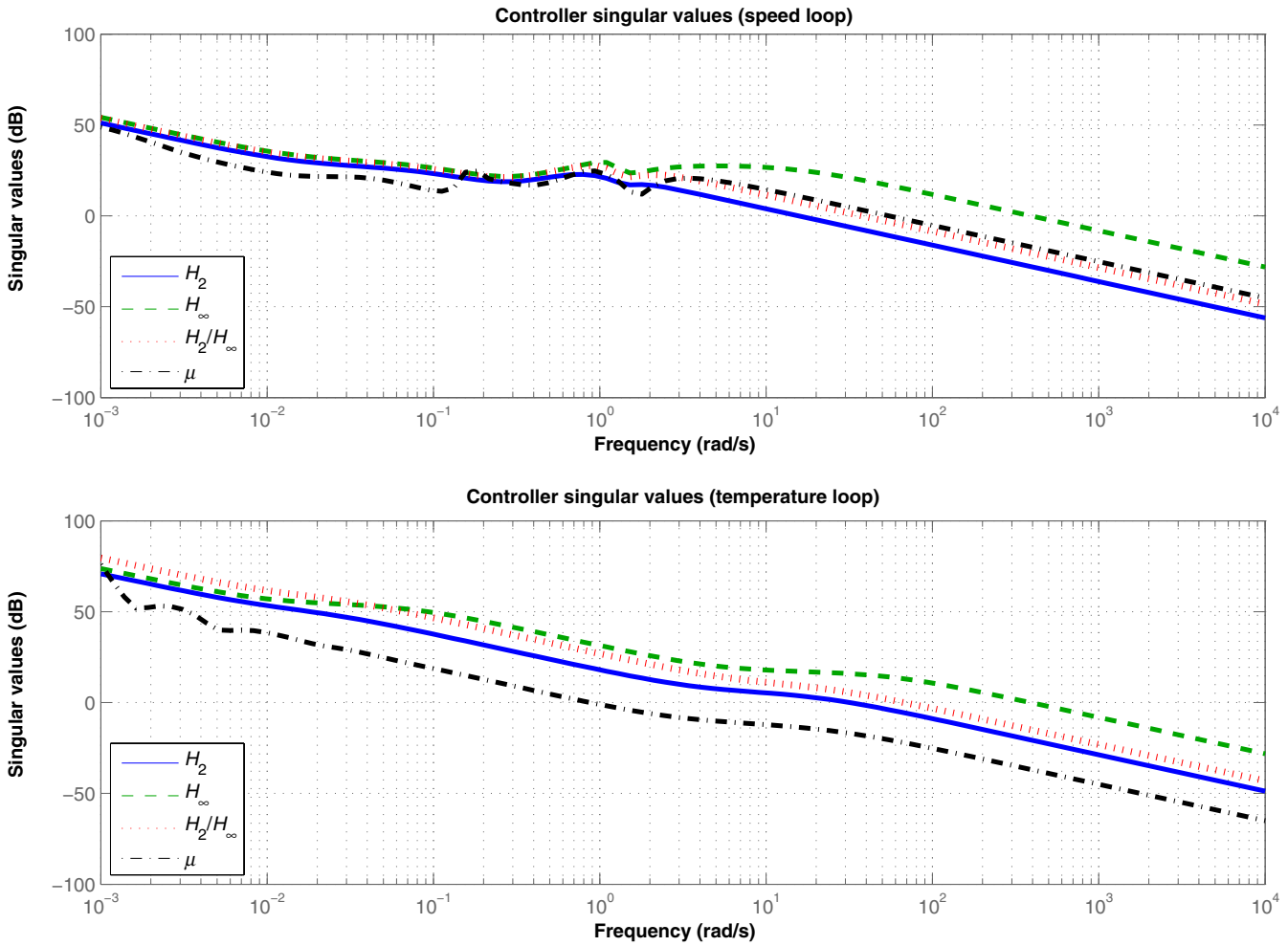

FIGURE 11 Speed and temperature controllers frequency responses

the performance analysis of the speed loop is relatively easier than that of the temperature loop. Analyzing the performance of this latter requires to take into account the effects of IGV control, fuel system, power, and speed outputs at the same time. In the case of IGV control and T_e, as Figures 14 and 15 show, IGV controller has an inverse effect on the temperature output and a control signal with a high overshoot and little rise time can lead to a better performance of the temperature response. In fact, at a fixed fuel flow, increasing the IGV signal increases the airflow to the power plant and decreases the gas temperature in the combustor. As can be seen in Figure 15, in the case of the H_2/H_∞ controller, any delay in opening the airflow can lead to an increase in the exhaust temperature beyond the reference T_r

In terms of tracking performance of the speed loop, as Figure 14 and Table 6 show, among all the robust controllers, H_∞ has the lowest deviations and output errors, while *μ-synthesis* has the highest deviations and output errors. The advantages of H_∞ are in direct connection with the RP (speed loop) presented in Figure 9 and Table 3. In the case of H_2 and H_2/H_∞ controllers, the fuel system acts to increase the fuel flow and compensate the sudden reduction in frequency output provided in Figure 14. As Figure 14 and Table 5 show, this can lead to an overshoot in power demand and output temperature. Increasing temperature over T_r moves the power plant from operating region *I* to *II* (Figure 4), where the IGV increases the airflow (Figure 14) to control the burning temperature.

For disturbance rejection capability, as Figure 15 and Table 7 show, among all the robust controllers, H_∞ shows more change and maximum deviation in terms of fuel flow (Figure 15) and power demand compared to the other controllers. The overshoot and deviation noted in Figure 15 can be explained by considering the high bandwidth of H_∞ in Figures 10 and 11, where, for H_∞, minimizing the frequency deviation has more priority than saving fuel flow. Besides, this overshoot in fuel flow can increase both temperature (Figure 15) and power output error (Table 7). As Figure 15 for IGV shows, H_2 and H_∞ provide the maximum deviation to maintain the output temperature below T_r This overshoot and deviation in Figures 14 and 15 are in close connection with the value of $W_{IGV} = 0.01$ and the best RP

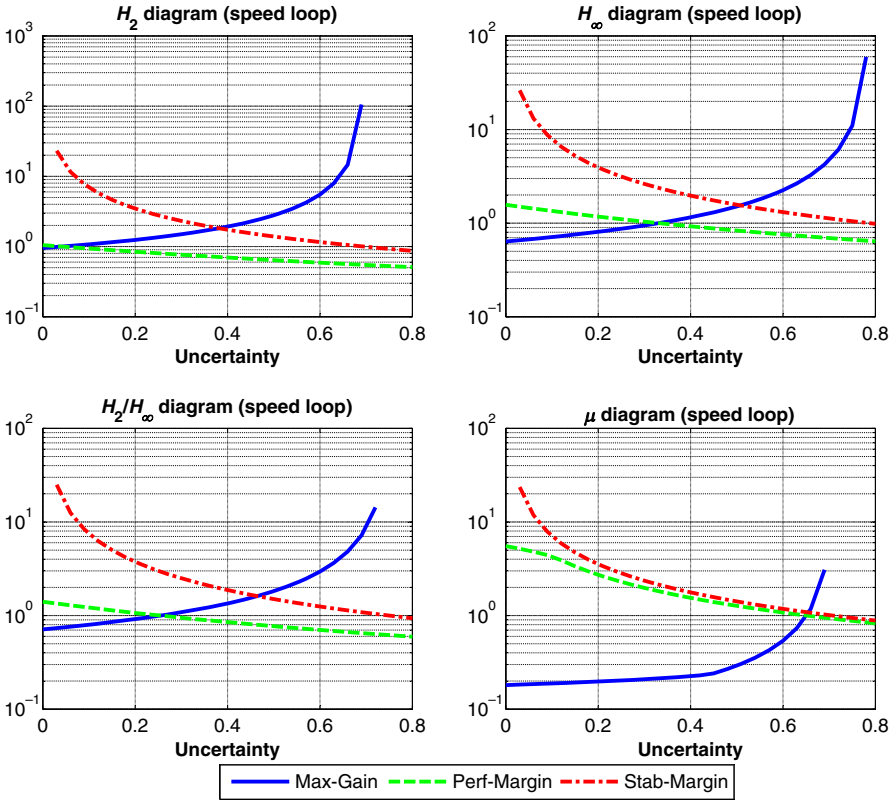

FIGURE 12 Maximum gain, performance margin, and stability margin for the speed loop

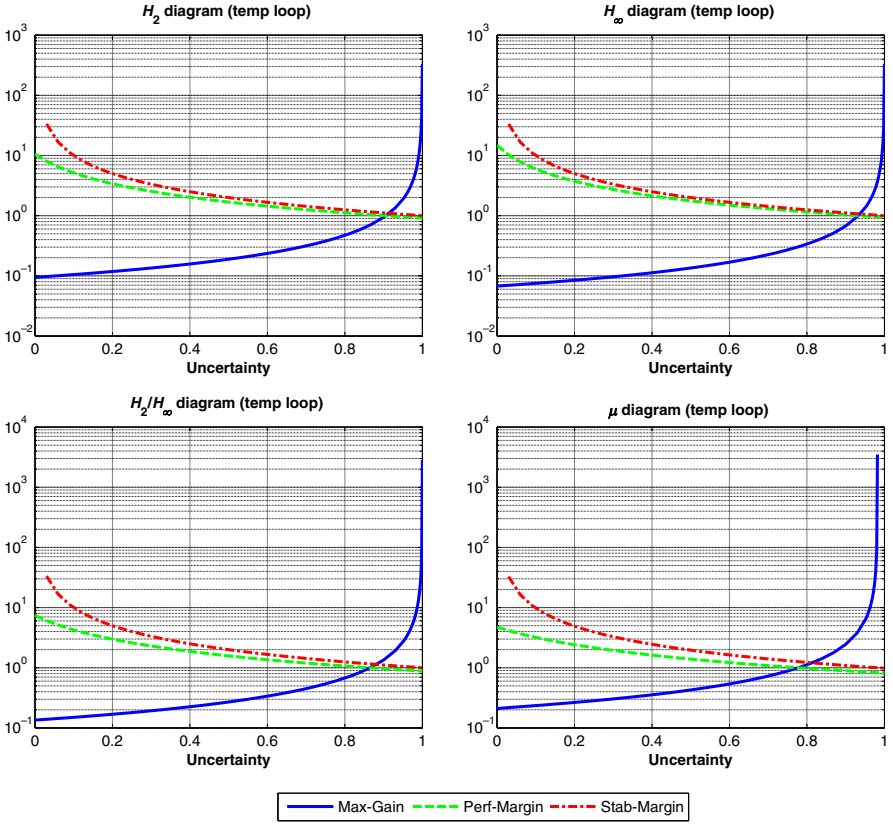

FIGURE 13 Maximum gain, performance margin, and stability margin for the temperature loop

in Figure 9 (temperature loop). Note that a lower weighing function (W_{IGV}) means more control energy for a better output performance.

Based on the simulation results and performance analysis provided in this section, we can conclude that among all the robust control approaches, H_∞ can offer the best stability and

TABLE 4 Maximum gain, stability margin, and performance margin for speed and temperature loops

Controller	Max-gain	Stab-margin	Stab-uncer	Perf-margin	Perf-uncer
Speed loop					
H_2	1.0-105.6	14.59	0.70	1.0	0.41
H_∞	0.67-59.68	**16.52**	**0.79**	1.45	0.33
H_2/H_∞	0.75-14.31	15.75	0.72	1.31	0.26
μ	**0.18-3.1**	15.72	0.69	**4.9**	**0.65**
Temperature loop					
H_2	**0.099-333.4**	**21.0**	**1.0**	7.0	0.91
H_∞	0.48-333.5	21	1.0	**8.6**	**0.93**
H_2/H_∞	0.14-2824	21.0	1	5.42	0.87
μ	0.22-3500	20.6	0.982	3.83	0.78

The bold values are the best simulation results.

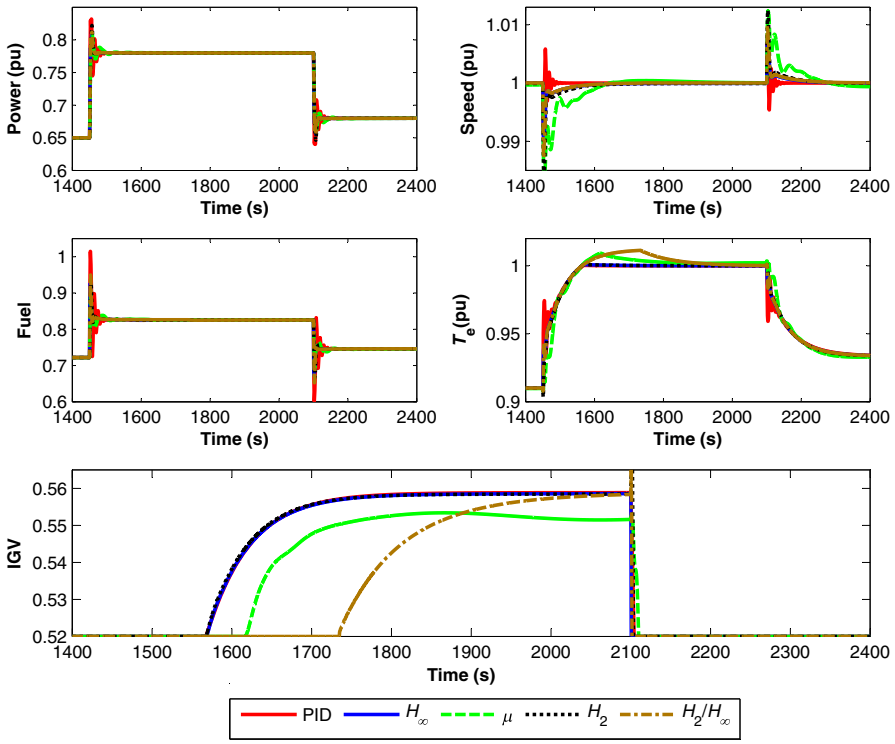

FIGURE 14 Output and control responses for H_2, H_∞, H_2/H_∞, μ-*synthesis*, and GTPP controllers

TABLE 5 Optimum time indices for H_2, H_∞, H_2/H_∞, μ-*synthesis* controllers and the main GTPP controller

Output	M_P (%)	T_r (s)	T_s (s)	Output	M_P (%)	T_r (s)	T_s (s)
H_2				H_∞			
Power	32.46	1.94	**62.53**	Power	24.25	1.40	62.69
T_e	1.06	**76.88**	**154.25**	T_e	0.96	79.24	155.59
H_2/H_∞				μ			
Power	24.53	1.44	62.88	Power	**21.18**	2.31	93.58
T_e	12.65	78.12	504.37	T_e	10.24	80.21	600
PID							
Power	40.06	**1.09**	82.81				
T_e	**0.35**	79.18	157.23				

The bold values are the best simulation results.

TABLE 6 Error indices for H_2, H_∞, H_2/H_∞, *μ-synthesis* controllers and the main GTPP controller

Error	ISE	IAE	ITSE	ITAE	Error	ISE	IAE	ITSE	ITAE
H_2					H_∞				
Power	8.76×10^{-01}	6.99	1248.48	9981	Power	$\mathbf{8.62 \times 10^{-01}}$	**6.81**	**1229.27**	**9721**
T_e	5.25×10^{-01}	7.39	752.91	10 719	T_e	5.09×10^{-01}	7.26	729.42	10 527
N	1.57×10^{-03}	0.33	2.30	507	N	7.39×10^{-04}	0.23	1.08	356
H_2/H_∞					μ				
Power	8.68×10^{-01}	6.89	1238.08	9834	Power	8.71×10^{-01}	7.14	1241.49	10 214
T_e	5.30×10^{-01}	9.53	764.67	14 449	T_e	5.92×10^{-01}	9.46	852.77	14 139
N	8.64×10^{-04}	0.21	1.26	323	N	4.94×10^{-03}	0.80	7.31	1226
PID									
Power	8.72×10^{-01}	7.14	1243.07	10 203					
T_e	$\mathbf{4.85 \times 10^{-01}}$	**6.90**	**694.59**	**9975**					
N	$\mathbf{2.84 \times 10^{-04}}$	**0.07**	**0.41**	**100**					

The bold values are the best simulation results.

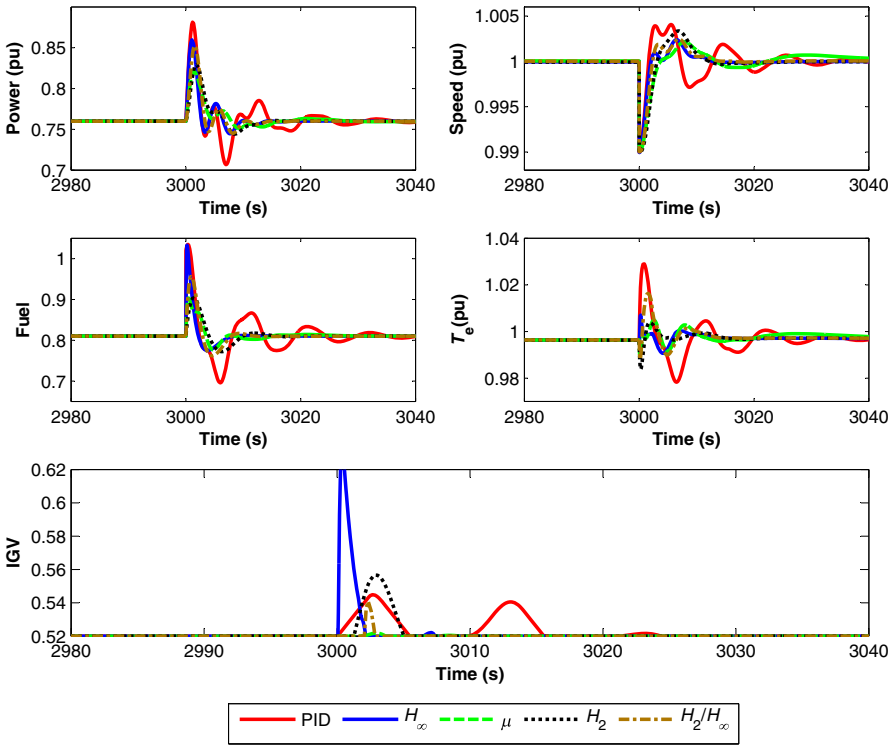

FIGURE 15 Output and control responses for 1% frequency drop

performance margins for the temperature loop, whereas for the speed loop, although H_∞ provides the best stability margin, it fails in the performance margin aspect compared to the *μ-synthesis* controller.

On the other hand, H_2 controller resulted in the worst stability and performance margins for the speed loop, whereas *μ-synthesis* yielded the worst stability and performance margins for the temperature loop. The tracking performance results showed that H_∞ and H_2 provided the best transient and steady-state behavior. Indeed, based on the results shown in Table 6, H_∞ can minimize the temperature and power outputs, which can save energy and cost and improve GTPP efficiency. The disturbance rejection analysis showed that both *μ-synthesis* and H_∞ can offer the minimum tracking error; however, when it comes to load frequency control, H_∞ should be the preferred solution.

6 | CONCLUSIONS

In this paper, H_2, H_∞, H_2/H_∞, and *μ-synthesis* controllers were designed and implemented for the speed and temperature control of a V94.2 gas turbine mounted in Damavand CCPP. The controllers were compared in terms of tracking

TABLE 7 ISE, IAE, ITSE, ITAE, mean, standard deviation (SD) and maximum deviation (MD) of output errors for 1% frequency drop

Method	ISE	IAE	ITSE	ITAE	Mean	SD	MD
H_2							
Power	9.88×10^{-03}	0.256	29.668	770	**0.749**	2.22×10^{-02}	6.95×10^{-02}
T_e	2.06×10^{-04}	**0.056**	0.618	170	0.996	2.94×10^{-03}	7.51×10^{-03}
N	1.88×10^{-04}	0.038	0.564	113	1.002	3.80×10^{-03}	3.35×10^{-03}
IGV	2.36×10^{-03}	0.084	7.100	252	0.518	6.93×10^{-03}	3.66×10^{-02}
Fuel	2.12×10^{-02}	0.400	63.693	1203	0.794	3.71×10^{-02}	9.35×10^{-02}
H_∞							
Power	1.34×10^{-02}	0.246	40.101	739	0.756	1.53×10^{-02}	9.97×10^{-02}
T_e	$\mathbf{1.55 \times 10^{-04}}$	0.057	**0.466**	171	0.995	$\mathbf{1.80 \times 10^{-03}}$	$\mathbf{1.06 \times 10^{-02}}$
N	$\mathbf{1.05 \times 10^{-04}}$	**0.023**	**0.316**	**69**	**1.000**	2.64×10^{-03}	2.38×10^{-03}
IGV	8.40×10^{-03}	0.112	25.213	337	0.517	1.43×10^{-02}	1.12×10^{-01}
Fuel	3.84×10^{-02}	0.355	115.115	1066	0.801	4.70×10^{-02}	2.23×10^{-01}
H_2/H_∞							
Power	1.27×10^{-02}	0.245	37.979	736	0.754	1.88×10^{-02}	9.25×10^{-02}
T_e	7.21×10^{-04}	0.094	2.166	284	**0.994**	3.77×10^{-03}	2.00×10^{-02}
N	1.43×10^{-04}	0.029	0.428	88	1.001	3.35×10^{-03}	2.47×10^{-03}
IGV	1.86×10^{-04}	0.011	0.560	32	0.520	1.78×10^{-03}	2.10×10^{-02}
Fuel	3.49×10^{-02}	0.427	104.671	1282	0.798	4.32×10^{-02}	1.46×10^{-01}
μ							
Power	$\mathbf{7.34 \times 10^{-03}}$	**0.242**	**22.037**	726	0.756	$\mathbf{1.38 \times 10^{-02}}$	$\mathbf{6.10 \times 10^{-02}}$
T_e	3.14×10^{-04}	0.088	0.946	264	0.995	2.24×10^{-03}	8.51×10^{-03}
N	1.52×10^{-04}	0.041	0.455	124	1.000	$\mathbf{2.00 \times 10^{-03}}$	$\mathbf{2.16 \times 10^{-03}}$
IGV	$\mathbf{2.86 \times 10^{-06}}$	**0.002**	**0.009**	**7**	**0.520**	$\mathbf{2.61 \times 10^{-04}}$	$\mathbf{1.82 \times 10^{-03}}$
Fuel	$\mathbf{1.46 \times 10^{-02}}$	0.335	43.787	1007	0.807	$\mathbf{1.94 \times 10^{-02}}$	$\mathbf{9.33 \times 10^{-02}}$
PID							
Power	2.54×10^{-02}	0.508	76.187	1528	0.756	2.18×10^{-02}	1.21×10^{-01}
T_e	2.51×10^{-03}	0.186	7.528	559	0.995	7.07×10^{-03}	3.26×10^{-02}
N	1.78×10^{-04}	0.052	0.535	157	1.001	3.47×10^{-03}	4.05×10^{-03}
IGV	2.26×10^{-03}	0.138	6.792	417	0.517	6.11×10^{-03}	2.49×10^{-02}
Fuel	1.05×10^{-01}	1.193	316.595	3590	**0.784**	7.59×10^{-02}	2.25×10^{-01}

The bold values are the best simulation results.

capability, robustness, and transient performance. They were shown to enhance the GTPP output responses for any frequency drop caused by changes in power demand. Additionally, the controllers were able to maintain the RS and performance of the closed-loop system in the presence of model uncertainties, quickly varying parameters, and unmodeled dynamics.

Our comparison study showed that, even if the H_∞ approach should be the preferred solution, the design goals for speed, power demand, and temperature outputs and the constraints on fuel flow and IGV control inputs cannot be satisfied at the same time using a single control approach. A compromise between the different objectives and control requirements is unavoidable and necessary.

ORCID

Vahab Haji Haji https://orcid.org/0000-0001-5186-1175

REFERENCES

1. Haji Haji V, Monje CA. Fractional order fuzzy-PID control of a combined cycle power plant using particle swarm optimization algorithm with an improved dynamic parameters selection. *Appl Soft Comput*. 2017;58:256-264.
2. Lalor G, Ritchie J, Flynn D, O'Malley MJ. The impact of combinedcycle gas turbine short-term dynamics on frequency control. *IEEE Trans Power Syst* 2005;20(3):1456-1464.
3. Mantzaris J, Vournas C. Modelling and stability of a single-shaft combined cycle power plant. *Int J Thermo*. 2007;10(2):71-78.

4. Kakimoto N, Baba K. Performance of gas turbine-based plants during frequency drops. *IEEE Trans Power Syst*. 2003;18(3):1110-1115.
5. Mantzaris J, Karystianos M,VournasC. *Comparison of Gas Turbine and Combined Cycle Models for System Stability Studies. MedPower Conference*. Thessaloniki, Greece; 2008.
6. Shalan H, Moustafa Hassan MA, Bahgat A. Comparative study on modeling of gas turbines in combined cycle power plants. In: *Proceedings of the 14th International Middle East Power Systems Conference (MEPCON10)*. Egypt: Cairo University; 2010:19-21.
7. Carmona S, Rios S, Peña H, Raineri R, Nakic G. Combined cycle unit controllers modification for improved primary frequency regulation. *IEEE Trans Power Syst*. 2010;25(3):1648-1654.
8. Kunitomi K, Kurita A, Tada Y, et al. Modeling combined-cycle power plant for simulation of frequency excursions. *IEEE Trans Power Syst*. 2003;18:724-729.
9. Saikia LC, Sahu KS. Automatic generation control of a combined cycle gas turbine plant with classical controllers using Firey algorithm. *Int J Elec Power*. 2013;53:27-33.
10. Jadhav SP, Chile RH, Hamde ST. Robust fractional-order controller using Bodes ideal transfer function for power plant gas turbine. *Int J Comput Appl*. 2014;88(16):1-7.
11. Iqbal M, Xavier RJ, Kanakaraj J. A neuro-fuzzy controller for grid-connected heavy-duty gas turbine power plants. *Turk J Elec Eng Comp Sci*. 2017;25:2375-2387.
12. Ghorbani H, Ghaffari A, Rahnama M. Constrained model predictive control implementation for a heavy-duty gas turbine power plant. *WSEAS Trans Syst Control*. 2008;3:507-516.
13. Mirrashid N, Rakhtala SM, Ghanbari M. Robust control design for air breathing proton exchange membrane fuel cell system via variable gain secondorder sliding mode. *Energy Sci Eng*. 2018;6(3):126-143.
14. Mseddi A, Ballois SL, Aloui H, Vido L. Robust control of a HESG for a wind energy application. *Electr Power Syst Res*. 2019;168:250-260.
15. Kafi MR, Chaoui H, Miah S, Debilou A. Local model networks based mixed-sensitivity H-infinity control of CE-150 helicopters. *Control Theory Technol*. 2017;15(1):34-44.
16. Najimi E, Ramezani MH. Robust control of speed and temperature in a power plant gas turbine. *ISA Trans*. 2012;51:304-308.
17. Kim S, Park J, Kang S, Young Kim P, Jin Kim H. A robust control approach for hydraulic excavators using μ-synthesis. *Int J Control Autom Syst*. 2018;16:1615-1628.
18. Liu M, Dong Z. Multiobjective robust H_2/H_∞ fuzzy tracking control for thermal system of power plant. *J. Process Contr*. 2018;70:47-64.
19. Kehlhofer R, Hannemann F, Rukes B, Stirnimann F. *Combined-Cycle Gas and Steam Turbine Power Plants*. Tulsa, OK: PennWell Corp.; 2009.
20. Ljung L. *System Identification: Theory for the User*. Upper Saddle River: Prentice Hall; 1999.
21. Ye F, Zhang W, Ou L H_2 consensus control of time-delayed multiagent systems: A frequency-domain method. *ISA Trans*. 2017;66:437-447.
22. Skogestad S, Postlethwaite I. *Multivariable Feedback Control Analysis and Design*. New York: John Wiley & Sons; 2001.
23. Haji HajiV, FekihA, MonjeCA. H∞ robust control design for a combined cycle power plant. In: *2019 IEEE PES GTD Grand International Conference and Exposition Asia (GTD Asia)*, 2019:384-389.
24. Khargonekar PP, Rotea MA. Mixed H_2/H_∞ control: A convex optimization approach. *IEEE Trans Autom Control*. 1991;36:824-831.
25. Krokavec D, Filasová A. On enhanced mixed H_2/H_∞ design conditions for control of linear time-invariant system. In: *17th International Carpathian Control Conference (ICCC)*; 2016:384-389.
26. Gu DW, Petkov PH, Konstantinov MM. *Robust Control Design with Matlab*. London Heidelberg New York Dordrecht: Springer; 2013.
27. Lari A, Khosravi A, Rajabi F. Controller design based on μ analysis and PSO algorithm. *ISA Trans*. 2014;53:517-523.
28. RowenWI. Simplified mathematical representation of single shaft gas turbines in mechanical drive service. In: *International Gas Turbine and Aeroengine Congress and Exposition Cologne*, Germany; 1992.
29. Haji Haji V, Monje CA. Fractional-order PID control of a chopper-fed DC motor drive using a novel Firey algorithm with dynamic control mechanism. *Soft Comput*. 2018;22:6135-6146.

How to cite this article: Haji Haji V, Fekih A, Monje CA, Fakhri Asfestani R. H_2, H_∞, H_2/H_∞, and *μ-synthesis* controllers for the speed and temperature control of a real gas turbine unit in a combined cycle power plant. *Energy Sci Eng*. 2019;7:2205–2222. https://doi.org/10.1002/ese3.425